



## Factorial Experimental Design for the Elimination of Cationic Dye Stuff from Aqueous Solution via a Novel Sediment–Alga–Silver Nanocomposite



CrossMark

Abeer A. M. El-Sayed, Safaa A. Abdel Ghani, Aida H. Shobier, Mohamed A. Aly-Eldeen\*

National Institute of Oceanography and Fisheries, NIOF, Egypt

### Abstract

One of the major concerns regarding water pollutants is dyes, which are prevalent in textile industrial wastewater. The present work studied the elimination of methylene blue (MB) dye from the aqueous medium through adsorption utilizing a novel, ecofriendly and cost-effective nanocomposite (sediment–alga–silver nanocomposite). The composite was prepared from the marine red alga *Jania rubens* and sediment enhanced by synthesized silver nanoparticles (AgNPs). It was distinguished by FTIR and SEM. A statistical model was used to evaluate the sorption efficiency of MB by the nanocomposite. The independent variables and their levels included a pH of (4–10), an adsorbent dosage (0.05–0.3 g/L), contact time (10–60 min) and an initial dye concentration (10–100 mg/L). The obtained data were analyzed statistically to define the most efficient combinations of independent parameters controlling the process. The maximum removal percentage (86.98%) was obtained at pH (8.5), adsorbent dosage (0.2375 g/L), contact time 47.5 min. and initial concentration (32.5 mg/L). The kinetic data correlated best with the pseudo-second-order model, while the isotherm data were better fitted to Freundlich and Langmuir isotherms. The calculated values of Temkin and Freundlich constants suggested a physical adsorption process of MB onto composite.

**Keywords:** Methylene blue; Response surface methodology; silver nanoparticles; nanocomposite adsorbent.

### 1. Introduction

The growing demand for water, coupled with the scarcity of natural water resources exacerbated by climate change and global warming, has led to increased efforts to reclaim wastewater for decontamination and reuse in domestic, agricultural, and industrial applications. This has prompted the strengthening of national and regional regulations governing the discharge of wastewater into the environment [1].

Indeed, wastewater contaminated with dyes is often linked to the textile industry. These dyes have serious environmental hazards if not fully controlled [2,3]. Their stable chemical structure allows them to persist in aqueous systems long-term, leading to reduced oxygen levels in aquatic life, generation of carcinogenic and mutagenic compounds with fatal impacts [4–6].

Methylene blue (MB) is indeed a significant dye used in various sectors, including pharmaceuticals and textiles industry. Its chemical properties, including being aromatic, cationic, and heterocyclic, make it versatile for dyeing processes. Despite its widespread use, MB poses health risks due to its stability in the human body and resistance to natural metabolic processes. Prolonged exposure to MB can lead to various health issues, including skin and gastrointestinal irritation, nausea, and even methemoglobinemia. These risks underscore the importance of effective wastewater treatment to mitigate the environmental and health impacts of dye contamination [7,8]. The allowable levels for methylene blue will vary by regulatory agency and municipality, but the Environmental Protection Agency (EPA) general guidelines recommend limit value of 0.2 mg/L [9]. The removal of dyes from water can be achieved through various processes, including precipitation and flotation [10–12], solvent extraction [13–15], catalytic and photocatalytic degradation [16–18], and sorption. The process of adsorption is widely utilized for the purification of water from toxic pollutants due to its effectiveness, cost-efficiency, versatility, and simplicity. Additionally, it can be utilized for both batch and continuous processes, even at extremely low contaminant concentrations, while producing minimal sludge. Sorption, using bio-based sorbents like nano-based materials [19], activated carbon (AC), biochar [1], composite materials including clay and clay minerals present a promising alternative for dye recovery from aqueous solutions [20]. Generally, Soil, including clays, sands, and sediments, have gained significant attention as alternative adsorbents in wastewater treatment. This is attributed to their numerous advantages, including low toxicity, abundant availability, high cation exchange capacity, and favourable textural properties [21]. These materials offer diverse adsorption capacities and can effectively remove dyes from wastewater, contributing to environmental remediation efforts.

\*Corresponding author e-mail: [m\\_niof@yahoo.com](mailto:m_niof@yahoo.com); (Mohamed A. Aly-Eldeen).

Received date 05 August 2024; revised date 02 September 2024; accepted date 16 September 2024

DOI: 10.21608/ejchem.2024.309694.10143

©2025 National Information and Documentation Center (NIDOC)

It is great to hear about the ongoing efforts to find effective and environmentally friendly adsorbents for purifying wastewater from toxic pollutants like dyes. Recently, a number of adsorbents have been used, such as: metal oxide-based adsorbents [22], dried seaweeds [23,24] Nanoadsorbent [25,26], which declared efficient competitor in the process of the MB dye removal.

On the other hand, green nanotechnology involves the production of nanomaterials using methods that minimize or eliminate harmful components throughout the manufacturing process [23].

Silver nanoparticles find wide-ranging applications and can be synthesized through various methods such as reduction in solution, chemical and photochemical reactions, electrochemical processes, sonochemical methods, microwave and laser technologies, as well as biological routes. Plant-mediated synthesis of silver nanoparticles is gaining prominence over chemical and microbial processes due to several advantages including cost-effectiveness, time efficiency, ease of accessibility, environmental friendliness, and low energy requirements [27]. Most of the researchers worldwide are interested in using biosynthesized silver nanoparticles by seaweed due to their availability and ease of harvesting [28].

Studies on dyes adsorption with various adsorbents employed a "one variable at a time" approach, assuming that the variables are independent. However, this assumption is often incorrect, and it becomes necessary to consider multiple factors simultaneously. In such cases, a full factorial analysis, which enables the assessment of more than one factor, is required [29]. The key advantages of this technique include obtaining insights into the effects of each variable and their relative importance, as well as identifying interactions among two or more components [29,30]. The evaluation of optimal adsorption conditions for dyes on various materials has been conducted using factorial design techniques by several studies [31–34].

The current study aims to leverage the advantages of nanoparticles, dried algae, and sediment through physical synthesis of sediment–alga–silver nanocomposite biosorbent for the elimination of MB from aqueous media. Response surface methodology (RSM) is applied to assess the impact of different variables and their interactions on the elimination of MB dye from aqueous solution. Additionally, the effectiveness of the synthesized composite in the purification process is evaluated.

## 2. Experimental

### 2.1. Pretreatment for sediment and algae biomass

Marine sediments and the red alga *Jania rubens* were collected from Abu-Qir Bay, Alexandria, Egypt. The marine alga was washed with seawater followed by distilled water (DW) to remove contaminants. The alga was air dried then oven dried at 45°C till a constant weight. The dried alga and sediments were ground to powder using a gate mortar then sieved using sieve of 63 µm mesh size then stored for further analyses [35,36].

### 2.2. Preparation of the algal extract

An aqueous extract of *J. rubens* was prepared by macerating 30 g of dried, sieved alga in 300 mL of DW and heated at 60 °C for 20 minutes followed by filtration using filter paper (Whatman №1) [37]. The resulting algal extract was then kept at 4 °C for further investigation.

### 2.3. Production of silver nanoparticles (AgNPs)

In the standard procedure for preparing AgNPs, 20 ml of *J. rubens* aqueous extract was mixed with 180 mL of a 0.01 M solution of silver nitrate (AgNO<sub>3</sub>) in a 250 mL conical flask. The mixture was slowly heated to 60 °C with stirring for 48 hours using a magnetic stirrer, to confirm complete reduction of the metal ions under dark conditions [37]. Additionally, the algal aqueous extract was used as a control [38]. The formation of Ag-NPs was confirmed visually by observing the colour change of the solution to brown. A UV-Visible spectrophotometry (Jenway SP-8001) at wavelengths between 200 and 800 nm was used to confirm the formation of AgNPs.

### 2.4. Preparation of sediment–alga–silver nanocomposite and its characterization

12.5 g of each sieved sediment and alga were mixed well and added to 50 mL of freshly prepared AgNPs solution. The sediment, algae and nanosolution mixture was kept overnight in shaker incubator. The mixture of sediment, algae, and nanosolution was stored in a shaker incubator overnight at 25 °C and 150 rpm. After centrifugation, the precipitated solid particles were air dried and kept for further study [27]. SEM (Joel- IT 200) and FTIR (Perkin Elmer Spectrum IR version 10.06.0) were used to examine the features of nanocomposite prior and following the sorption procedure.

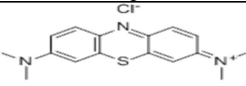
### 2.5. Measurement of pH<sub>pzc</sub> (Point of zero charge):

The pH of the dye solutions was adjusted to a range between 2 and 12 employing 0.1M HCl and 0.1M NaOH solutions measured with a pH meter (Consort C860, Belgium). Following that, 0.1 g of nanocomposite was then added to each solution, and the mixtures were agitated for 24 hours at 200 rpm. The final pH of each solution (pH<sub>f</sub>) was then determined. The diagram of the pH<sub>f</sub> of the solution vs its initial (pH<sub>i</sub>) value was plotted. The pH<sub>pzc</sub> of the nanocomposite was the point where the curves intersected at zero [39].

### 2.6. Dye adsorption study

The chemical structure and properties of MB dye were listed in Table 1. A stock solution of MB (500 mg/L) was prepared in DW and diluted to obtain the desired concentrations of dye solutions. The pH of obtained solutions was adjusted using 0.1 M HCl and 0.1 M NaOH solutions.

**Table 1:** Chemical structure and properties of MB dye

Property	Description
Chemical structure	
Molecular Formula	C <sub>16</sub> H <sub>18</sub> ClN <sub>3</sub> S
Type of dye	Cationic dye
UPAC Name	[7-(dimethylamino)phenothiazin-3-ylidene]-dimethylazanium;chloride
Molecular weight	319.85
(λ <sub>max</sub> )	661 nm
Color	Dark blue crystals or powder
Solubility	Soluble in water or alcohol

The removal experiments were achieved in batch mode at room temperature. For a typical adsorption experiment, the defined weight of the composite was mixed with 100 mL of MB solutions and agitated on a mechanical shaker at 200 rpm. After required contact times (t), the solutions were centrifuged at 4000 rpm for 10 min. A calibration curve was performed, and the dye concentrations in the supernatant were measured using a UV-Vis spectrophotometer at 662 nm. To investigate the adsorption isotherm and kinetics models, the study of the initial concentration effect was conducted in different dye concentrations of 10, 32.5, 55, 77.5 and 100 mg/L, under the following reaction conditions: pH, 8.5; adsorbent dose, 1 g/100 mL; room temperature; contact time, 60 min; speed of agitation, 200 rpm. Using the equations shown in Table 2, the quantity of dye adsorbed at equilibrium (q<sub>e</sub>) or at a certain moment in the sorption process (q<sub>t</sub>) (mg/g) and the removal percentage (removal %) of MB dye were calculated [40].

### 2.7. Central composite design

The Central Composite Design (CCD) using design expert software was used to assess the influence of four independent factors (pH, adsorbent dose, contact time, and initial dye concentration). Experiments, including 16 factorial points, 8 axial points, and 6 replicate points. Repetition points help to avoid experimental errors in the design. Levels of the selected parameters (-2, -1, 0, 1, and +2) are shown in Table 3.

The adsorption experiments were conducted randomly at the selected four different levels of independent variables coded as +2, +1 and -1, -2 for high and low values with six central points. All probable combinations of the variables were employed, and then a coded matrix was generated by software as listed in Table 4. The total number of the experiments was estimated according to Eq. (1) [41].

$$N = 2^{2n} + 2n + n_c \quad (\text{Eq. 1})$$

where N represents the total trial numbers, n= the number of parameters and n<sub>c</sub>= the replicated number of center points which was 6 points in the current study.

At the end of the experiments, the dye removal efficiency regression model is expressed by the following formula (Eq. 2) [42]:

$$Y = \beta_0 + \sum_{i=1}^m \beta_i X_i + \sum_{i < j}^m \beta_{ij} X_i X_j + \sum_{i=1}^m \beta_{ii} X_i^2 \quad (\text{Eq. 2})$$

where Y indicates dependent variable of response, X<sub>i</sub> and X<sub>j</sub> are independent variables and β<sub>0</sub>, β<sub>i</sub>, β<sub>ij</sub>, and β<sub>ii</sub> are the intercept term, linear, quadratic, and interaction effects, respectively. The validity of suggested model was evaluated using different statistical parameters i.e., coefficient of determination (R<sup>2</sup>), adjusted R<sup>2</sup> (R<sup>2</sup> adj) and predicted R<sup>2</sup> (R<sup>2</sup> pred) [57].

## 3. Results & Discussions

### 3.1. Description of silver nanoparticles (AgNPs)

#### 3.1.1. Visual examination:

The AgNPs were generated by reacting AgNO<sub>3</sub> solution with algal aqueous extract at a temperature of 60 °C with stirring. The control extract remained without change even after 48 hrs of heating. The reduction process of AgNO<sub>3</sub> was optically validated by a transformation of yellowish-brown to reddish-brown color after 30 minutes, then the brown color intensity was elevated in synergistic with the heating time [28].

**Table 2:** Equations of applied isotherm and kinetic models and their calculated parameters values for adsorption of MB onto sediment–alga–silver nanocomposite

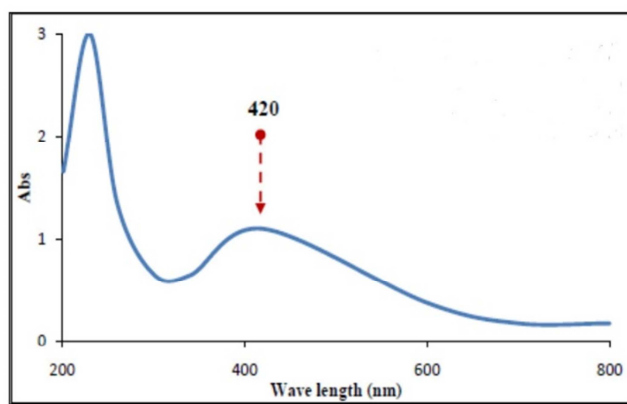
Model	Linear equation	Parameter	Parameter value	R <sup>2</sup>	Reference
<b>Isotherm models</b>					
	$q_e = \frac{C_o - C_e}{m} \times v$ $q_t = \frac{C_o - C_t}{m} \times v$ $R \% = \frac{C_o - C_e}{C_o} \times 100$	$q_e$ : the sorption equilibrium capacity (mg/g) $C_o$ : the initial concentration of Cr(VI) (mg/L) $C_e$ : the equilibrium sorption concentration of Cr(VI) (mg/L) $m$ : the weight of biosorbent (g) $v$ : the volume of hexavalent chromium Cr(VI) solution (L) $q_t$ : the sorption capacity at a certain moment (mg/g) R %: removal percentage			[43]
Langmuir	$\frac{1}{q_e} = \frac{1}{q_m} + \frac{1}{bq_m C_e}$ $R_L = \frac{1}{1 + bC_o}$	$q_m$ : the maximum adsorption capacity (mg g <sup>-1</sup> ). $b$ : constant $R_L$ : the separation factor. When $R_L = 0$ the sorption process is irreversible; $R_L < 1$ , favorable; $R_L = 1$ , linear; $R_L > 1$ unfavorable.	$q_m = 7.83$ $b = 0.40$ $R_L = (0.02 - 0.2) < 1$	0.9915	[44,45]
Freundlich	$\ln q_e = \frac{1}{n} \ln C_e + \ln k_f$	$k_f$ and $\frac{1}{n}$ are constant that depend on the properties of the adsorbate and adsorbent	$n = 1.03$ $\frac{1}{n} = 0.97$ ; $k_f = 0.1029$	0.9991	[46,47]
Dubinin–Radushkevich (D-R)	$\ln q_e = \ln q_0 - k' \varepsilon^2$ $\varepsilon = RT \ln \left( 1 + \frac{1}{C_o} \right)$ $E = \frac{1}{(2k')^{1/2}}$	$\varepsilon$ : Polanyi potential $R$ : universal gas constant (8.314 J/mol K) $T$ : temperature in Kelvin (K) $k'$ : constant of the adsorption energy $E$ : adsorption energy	$E = 0.05 \text{ kJ/mol}$ $q_o = 7.979$	0.9116	[48,49]
Temkin	$q_e = B \ln K_t + B \ln C_e$ $B = \frac{RT}{b}$	$B$ : constant related to the heat of adsorption $b$ : Temkin isotherm constant (J/mol) $K_t$ : = Temkin isotherm equilibrium binding constant (L/g)	$B = 4.905$ $b = 0.493 \text{ kJ/mol}$ $K_t = 0.054$	0.9652	[50–52]
<b>Kinetic models</b>					
Pseudo-first-order	$\ln(q_e - q_t) = \ln q_e - k_1 t$	$k_1$ : Rate constant	$k_1 = 0.006 - 0.112$ $q_{(\text{exp})} = (0.053 - 0.385)$ $q_{(\text{cal})} = (0.908 - 8.197)$	0.0399–0.2826	[53,54]
Pseudo-second-order	$\frac{t}{q_t} = \frac{1}{k_2 q_e^2} + \frac{1}{q_e}$	$k_2$ : Rate constant	$k_2 = 0.015 - 1.21$ $q_{(\text{exp})} = (0.899 - 8.222)$ $q_{(\text{cal})} = (0.908 - 8.197)$	(0.9994–1.000)	[55,56]

**Table 3:** Experimental levels and range of independent factors in response surface methodology design for Methylene blue dye removal using nanocomposite

variable	-2	-1	0	1	+2
pH-(A) ( $X_1$ )	4	5.5	7	8.5	10
Adsorbent dose (g/l)-(B) ( $X_2$ )	0.05	0.1125	0.175	0.2375	0.3
Initial Conc. (ppm)- (C) ( $X_3$ )	10	32.5	55	77.5	100
Contact time (min.) -(D) ( $X_4$ )	10	22.5	35	47.5	60

### 3.1.2. Ultraviolet-Visible spectrum

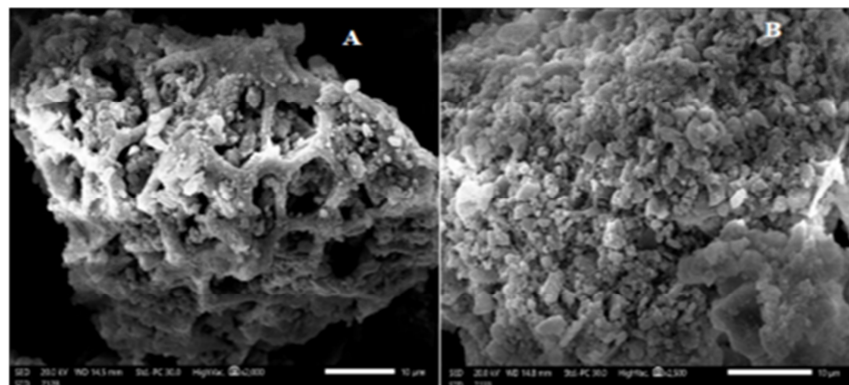
The UV-Vis spectrum is a confirmation method for the AgNPs synthesis, identified by the appearance of a surface plasmon resonance (SPR) vibration band absorbed at a definite wavelength. Fig. (1) reveals that after 48 hrs, the SPR vibration appeared as a broad band at 420 nm, which is in agreement with Bhuyar et al. [28].

**Figure 1:** UV-Visible spectrophotometer of AgNPs from algal extract.

## 3.2. Chemical features of sediment–alga–silver nanocomposite before and after adsorption

### 3.2.1. Morphological surface of the nanocomposite

Fig. (2A, B) shows the exterior surface and morphology of the sediment–alga–silver nanocomposite pre and post sorption of MB. The external surface of the nanocomposite before adsorption is characterized by roughness, with several thick, calcified walls of diverse chambers of *J. rubens*, (like bee cells), with varying sizes and types of uneven sediment particles scattered heterogeneously. The Ag-nanoparticles have a spherical shape and a uniform distribution with no aggregation, which increases the surface area, and hence enhances the uptake of MB dye (Fig. 2A) [58–60]. At this point, after adsorption, MB cohered to the nanocomposite surface; and the texture of the surface became soft and homogenous (Fig. 2B) [61].

**Figure 2:** Morphological images of sediment–alga –silver nanocomposite (A) before and (B) after the adsorption of methylene blue.

**Table 4:** Experimental design matrix of four independent variables affecting Methylene blue dye removal using nanocomposite

Run	A: pH	C: adsorbent (g/l)	B: Time (min.)	D: initial conc. (ppm)
1	-1	1	-1	-1
2	0	0	2	0
3	0	0	0	0
4	0	2	0	0
5	0	0	0	0
6	0	0	0	0
7	1	1	1	-1
8	1	1	1	1
9	-2	0	0	0
10	1	-1	-1	1
11	0	-2	0	0
12	-1	-1	-1	1
13	0	0	0	0
14	1	1	-1	-1
15	0	0	0	-2
16	1	-1	1	1
17	-1	-1	1	-1
18	-1	-1	1	1
19	0	0	-2	0
20	-1	1	1	1
21	1	-1	1	-1
22	1	-1	-1	-1
23	2	0	0	0
24	1	1	-1	1
25	0	0	0	0
26	-1	-1	-1	-1
27	0	0	0	0
28	0	0	0	2
29	-1	1	-1	1
30	-1	1	1	-1

### 3.2.2. Surface functional groups of nanocomposite

The results of FTIR spectra of sediment–alga–silver nanocomposite, pre and after MB biosorption, are shown in Table 5 and Fig. (3A, B).

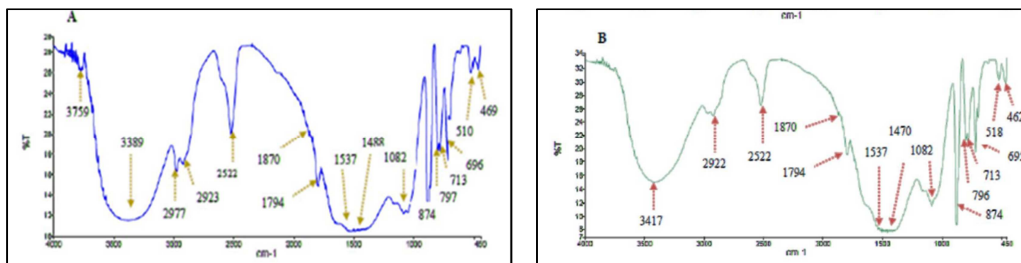


**Figure 3:** FTIR of sediment-alga-silver nanocomposite (A) pre and (B) post the adsorption of MB dye.

For pre sorption of the dye stuff, the small peak at  $3759\text{ cm}^{-1}$  signifies the presence of an N–H group, which could be attributed to the amino group in the alga or asymmetric O–H stretching of polyphenols in the nanocomposite [62,63]. The large, strong broad peak at  $3389\text{ cm}^{-1}$  corresponds to the O–H stretching vibration of phenolic groups (a protective coating on the AgNPs) or polysaccharides in *J. rubens* [35,62,64].

**Table 5:** Surface functional groups monitored on sediment–alga–silver nanocomposite pre and after sorption process

Sediment–alga–silver nanocomposite			
Before sorption $\text{cm}^{-1}$	After sorption $\text{cm}^{-1}$	Status of peaks	Bands indicating functional groups
3759	-	Disappeared	asymmetric O-H stretching or –NH group
3389	3417	Shifted	O-H stretching
2977	-	Disappeared	C-H stretching
2923	2922	Shifted	Aliphatic C-H stretching or -CH <sub>3</sub> & -CH <sub>2</sub> stretching
2522	2522	Fixed	Thiol S–H stretch
1870	1870	Fixed	C-OH stretching
1794	1794	Fixed	-NH R' or Calcite (CaCO <sub>3</sub> )
1537	1537	Fixed	N-H bending of amide (II)
1488	1470	Shifted	Symmetric R-C-O-O' stretching or C-C stretch aromatic ring
1082	1082	Fixed	Si-O-Si stretching vibration
874	874	Fixed	Calcite (CaCO <sub>3</sub> )
797	796	Shifted	Feldspar (-AlSi <sub>3</sub> O <sub>8</sub> )
713	713	Fixed	N-H vibration of fatty acid
696	695	Shifted	Fe-O stretch
510	518	Shifted	Quartz or silica (SiO <sub>2</sub> )
469	462	Shifted	Feldspar (-AlSi <sub>3</sub> O <sub>8</sub> )

The medium, slightly intense band at  $2977\text{ cm}^{-1}$  resembles asymmetric C–H stretching in soil alkanes [65]. The assimilation weedy band at  $2923\text{ cm}^{-1}$  may be attributed to stretching symmetric aliphatic vibration of the C–H or –CH<sub>3</sub> and –CH<sub>2</sub> of the secondary amines or the chlorophyll compounds, respectively in *J. rubens* [35]. The sharp and robust signal at  $2525\text{ cm}^{-1}$  coincides with the thiol S–H stretch in red seaweeds [59]. The weak wave at  $1870\text{ cm}^{-1}$  could be due to a C–OH stretching bond in the soil [66]. The moderate and partially sharp signal at  $1794\text{ cm}^{-1}$  belonged to (–NHR') secondary amide [67] or the calcite (CaCO<sub>3</sub>) compound in the sediment [68]. The existence of an absorption peak at  $1537\text{ cm}^{-1}$  may indicate an N–H bending type of amide (II) bonded in the tested red algal species [59]. The small peak at  $1488\text{ cm}^{-1}$  points to the symmetric R–COO– (carboxylate group) stretching [64,69] or the C–C stretch aromatic ring [70]. The presence of soaking up bands around regions ( $1082\text{--}469\text{ cm}^{-1}$ ) except peak ( $713\text{ cm}^{-1}$ ) is considered the imprint of soil composition, where  $1082$ ,  $874$ ,  $696$ ,  $510$ , ( $797$  &  $469$ )  $\text{cm}^{-1}$  signals are assigned to the Si–O–Si stretching vibration, calcite (CaCO<sub>3</sub>), Fe–O stretch, quartz or silica (SiO<sub>2</sub>), and feldspar (–AlSi<sub>3</sub>O<sub>8</sub>, aluminium silicate), respectively [68,71]. While the attendance of N–H vibration of fatty acid in *J. rubens* species at split medium and sharp band ( $713\text{ cm}^{-1}$ ) [35]. The appearance of previous peaks of pre-MB sorption is evidence for the formation of sediment–alga–silver nanocomposite (Fig. 3A).

After the dye sorption, the sorption process of MB on the nanocomposite surface results in considerable changes in the strength, location, and fixation of peaks, as well as the disappearance or appearance of new peaks, as shown in Table 5 and Fig. (3B). These alterations indicate that the peaks are engaged in the sorption process and that the MB material interacts with functionalities on the surface of nanocomposites through ion-dipole, electrostatic, H–bond, and van der Waals bond interactions [39,72]. The disappearance of the peak at  $3759\text{ cm}^{-1}$  indicates that the N–H group is involved in the sorption process. While the O–H band (phenolic or polysaccharide compounds) was lowered and considerably transferred to  $3417\text{ cm}^{-1}$ , the other six signals were marginally moved to  $2922$ ,  $1470$ ,  $796$ ,  $695$ ,  $518$ , and  $462\text{ cm}^{-1}$ . On the other hand, several bands remained constant, while the lone peak ( $2977\text{ cm}^{-1}$ ) faded, indicating a productive interaction between numerous common functional groups in the nanocomposite texture and the dye [63].

### 3.2.3. The $\text{pH}_{\text{pzc}}$ of nanocomposite

Fig. (4) shows that the  $\text{pH}_{\text{pzc}}$  of sediment–alga–silver nanocomposite is 9.0 which means that at the pH of 9.0, the positive and negative charges on the texture of the nanocomposite are equivalent to zero charges. At the  $\text{pH}_{(\text{solution})} > 9.0$ , the surface of the nanocomposite has negative charges, so the adsorption of MB (cationic dye) will be preferred, and contrariwise for anionic dye [39]. From the present study, the maximum removal of MB occurred at pH 8.5, which is close to the  $\text{pH}_{\text{pzc}}$  value of 9. This indicates that the adsorbent possesses negative charges, enhancing the elimination of the adsorbate.

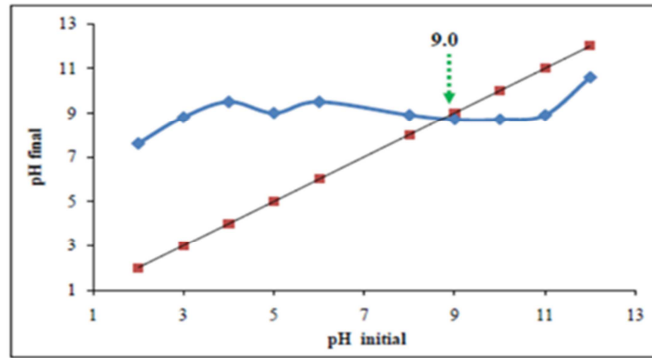


Figure 4:  $\text{pH}_{\text{pzc}}$  diagram of sediment–alga–silver nanocomposite.

### 3.3. Adsorption isotherm

The adsorption isotherm provides crucial insights into how the adsorbate interacts with the adsorbent under different conditions. It aimed at assessing the adsorbent materials' capacity, thereby informing the design and optimization of adsorption processes for efficient adsorbate removal.

In this study, linear regression equations of Langmuir, Freundlich, Dubinin-Radushkevich (D-R), and Temkin adsorption isotherms were implemented to investigate the adsorption of MB onto sediment–alga–silver nanocomposite. The values of correlation coefficient of each isotherm are compared to decide which of these isotherms can be followed. Table 2 summarizes the equations used and the resultant values of parameters. The observed data of MB adsorption onto the nanocomposite are fitted to the investigated models with varying degrees (Fig. 5a–d).

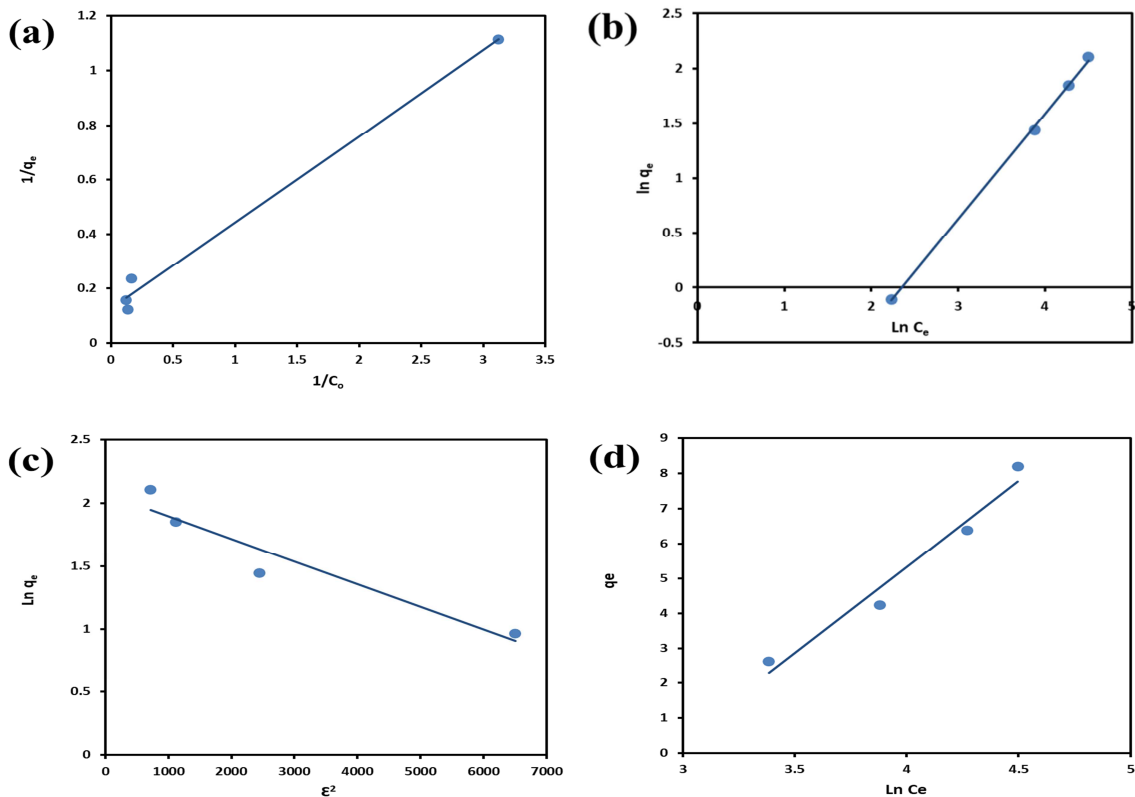


Figure 5: The plots of (a) Langmuir, (b) Freundlich, (c) Dubinin–Radushkevich (D-R) and (d) Temkin adsorption isotherm models for the adsorption of MB onto sediment–alga–silver nanocomposite at different concentrations.



The Langmuir model states that the adsorption process begins when a uniform monolayer of dye compounds forms on the texture of adsorbent. It suggests that only specific active sites on the adsorbent surface are occupied uniformly because the surface is assumed to be homogeneous. The Langmuir constants values of  $q_m$  and  $b$  were (7.83 mg/g) and (0.40), respectively. The value of  $q_m$  was found to be greater than that reported in the literature for other adsorbents: leaf powder of neem; 5.87 mg/g [73], corncob activated carbon; 0.84 mg/g [74], fly ash; 5.57 mg/g [74], and  $Mn_3O_4$ - $Bi_2O_3$  composite; 3.12 mg/g [22] (Table 6). The calculated  $R_L$  values of MB adsorption onto composite ranged from 0.02 to 0.20, reflecting a favourable isotherm model.

**Table 6:** Comparison of the adsorption capacity of different adsorbents for MB removal from aqueous solutions

Adsorbents	Sorption capacity $q_m$ (mg/g)	References
Neem leaf powder	5.87	[73]
Corn cob based activated carbon	0.84	[74]
Fly ash	5.57	[74]
Natural clay	15.4	[20]
$Mn_3O_4$ - $Bi_2O_3$ composite	3.12	[22]
Nano composite	7.83	Present study

The Freundlich model is employed to explore the heterogeneous nature of the adsorbent surface, considering both monolayer and multilayer adsorption phenomena.  $K_F$  and “ $n$ ” values obtained from this isotherm are shown in Table 2. When the heterogeneity factor ( $n$ ) value falls between 1 and 10, a good adsorption process is indicated, it also the nature of adsorption is linear at  $n=1$ , chemisorption at  $n<1$  or physisorption at  $n>1$  [75]. The higher heterogeneity of surface related to the value of  $1/n$  ( $1 > 1/n \approx 0$ ) [76–78]. In the present work, the values of  $n$  and  $1/n$  are 1.03 and 0.97, respectively, which suggests that the adsorption is physisorption and favourable. As shown in Table 2, it is evident that the Freundlich model provides a better fit to the experimental data compared to the Langmuir model. This is supported by the higher correlation coefficient ( $R^2 = 0.9991$ ) for the Freundlich model, whereas the Langmuir model exhibits a lower correlation coefficient ( $R^2 = 0.9915$ ).

The removal of MB using the nanocomposite was investigated by linear equation of Temkin model (Table 2) and the plot is demonstrated in Fig. (5d). This isotherm provides insights into the impact of indirect interactions between the nanocomposite and dye solution on the adsorption process [79]. The measured values of Temkin constants, with  $b = 0.49$  kJ/mol and  $K_t = 0.054$  L/g indicates a physical adsorption process of MB onto the nanocomposite

The Dubinin-Radushkevich (D-R) model describes the ion exchange mechanism and the chemical and physical forces involved in adsorption. If the value of the parameter  $E$  is  $< 8$  kJ/mol, physical adsorption dominates, while chemical adsorption prevails if the  $E$  value is  $> 8$  [80]. From this study, the energy of adsorption was less than 8 ( $E = 0.05$  kJ/mol), which suggests a physical adsorption. Moreover, the obtained maximum adsorption capacity ( $q_m$ ) was 7.98 mg/g which is close to the value obtained from Langmuir model.

Based on  $R^2$  value (Table 2), the investigational data were well adjusted by Freundlich  $>$  Langmuir  $>$  Temkin  $>$  Dubinin-Radushkevich (D-R).

### 3.4. Adsorption kinetics

The pseudo-first-order and pseudo-second-order kinetic models were employed to analyze the rate uptake of MB molecules onto the surface of nanocomposite. The validation of these models was depended upon the correlation coefficient ( $R^2$ ), providing insights into the kinetics of the adsorption process [81].

Table 2 presents the parameters of the models, along with their linear equations and corresponding correlation coefficients. It was observed that the adsorption of MB onto the nanocomposite did not align well with the pseudo-first-order kinetic model (Fig. 6a). However, the estimated equilibrium adsorption capacity ( $q_e$ ) obtained from the second-order model closely matched the experimental ( $q_e$ ) values, with correlation coefficients ( $R^2$ ) exceeding 0.999 for all dye initial concentration. This indicates the suitability of the second-order kinetics model and confirms the second-order nature of the biosorption process of MB onto the nanocomposite (Fig. 6b). Additionally, it was noted that the rate constant ( $k_2$ ) decreased with the increasing concentration of MB initially introduced.

### 3.5. Central composite design studies

In the current study, the elimination percentage of MB from contaminated solution under the influence of four independent factors was examined using experimental design software. Fitting statistics of generated models by the program including the suggested one are given in Table 7. Based on the model with the highest order polynomial where the additional terms are significant, and the model without aliasing, the quadratic model was chosen for the current investigation.

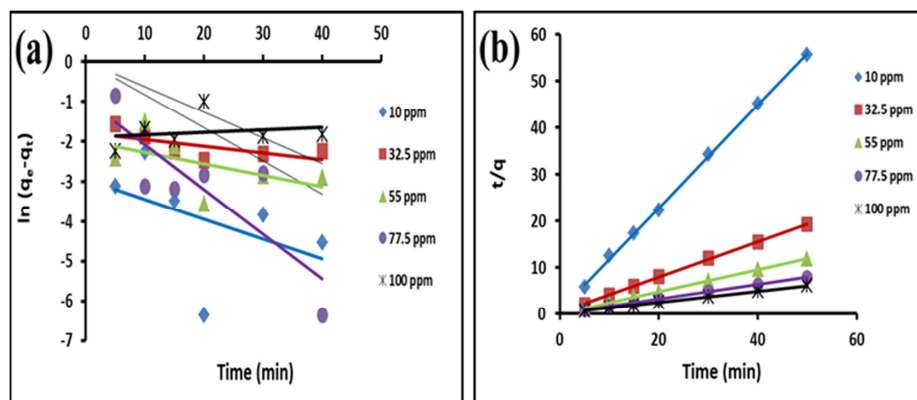


**Figure 6:** Plots of pseudo-first-order (a), pseudo-second-order (b) kinetic models for MB sorption by sediment–alga–silver nanocomposite.

**Table 7:** Model fitting statistics

Source	Sum of Squares	df	Mean Square	F-value	p-value	
Mean vs Total	1.82E+05	1	1.82E+05			
Linear vs Mean	1473.42	4	368.36	16.5	< 0.0001	
2FI vs Linear	85.03	6	14.17	0.5693	0.7497	
<b>Quadratic vs 2FI</b>	<b>377.33</b>	<b>4</b>	<b>94.33</b>	<b>14.8</b>	<b>&lt; 0.0001</b>	<b>Suggested</b>
Cubic vs Quadratic	70.12	8	8.77	2.4	0.1323	Aliased
Residual	25.51	7	3.64			
Total	1.84E+05	30	6141.51			

The ANOVA results for the suggested quadratic model describing the removal process under the effect of independent variables are listed in Table 8. These results give us an indication about the suitability of suggested quadratic model for representation of the removal process at the studied conditions.

The suggested model is significant, as indicated by an F-value of 21.69. There is only a 0.01% chance that an F-value this large could occur due to noise. However,  $p$ -values < 0.0500 revealed that model terms are significant [82]. In this case A, B, D, AD, BC and  $B^2$  are significant model terms, while values > 0.1000 indicate the un-significantly of model terms.

Lack of Fit F-value is 1.43, revealing that the lack of fit is statistically insignificant with respect to the pure error. A non-significant lack of fit is acceptable. On other hand, the  $p$ -value for lack of fit (0.3627) is higher than 0.05, indicating that the model fits the experimental results, and the independent process variables have a significant impact on the response [83].

According to the experimental design, the results were examined and the removal efficiency of methylene blue using the nanocomposite was obtained. The final quadratic equation of the model suggested by software that describes the removal process is given in Eq. 3 in terms of coded independent factors.

$$\text{Removal(\%)} = 82.52 + 2.32A + 6.43B - 0.7722C + 3.75D - 0.2783AB + 0.7023AC - 1.43AD + 1.35BC - 0.9033BD - 0.2177CD - 0.7892A^2 - 3.70B^2 - 0.5846C^2 - 0.6574D^2 \quad (\text{Eq. 3})$$

Fit statistics of the suggested models are given in Table 7. From this table we observed that regression coefficient  $R^2$  (0.9529) which ensures the better and goodness of the suggested model [41].

Data in Table 9 show that predicted  $R^2$  (0.7814) is in reasonable agreement with the Adjusted  $R^2$  (0.909); because the difference of each other approximately within 0.2.

**Table 8:** ANOVA results for Quadratic model describing the responses variation

Source	Sum of Squares	df	Mean Square	F-value	p-value	
<b>Model</b>	1935.78	14	138.27	21.69	< 0.0001	significant
A-pH	129.67	1	129.67	20.34	0.0004	
B-Dose	992.58	1	992.58	155.6	<	
C-Init. Conc	14.31	1	14.31	2.24	0.1548	
D-Time	336.87	1	336.87	52.84	<	
AB	1.24	1	1.24	0.194	0.6655	
AC	7.89	1	7.89	1.24	0.2834	
AD	32.91	1	32.91	5.16	0.0382	
BC	29.17	1	29.17	4.58	0.0493	
BD	13.05	1	13.05	2.05	0.1729	
CD	0.7582	1	0.7582	0.118	0.735	
A <sup>2</sup>	17.09	1	17.09	2.68	0.1224	
B <sup>2</sup>	375.16	1	375.16	58.84	<	
C <sup>2</sup>	9.37	1	9.37	1.47	0.2441	
D <sup>2</sup>	11.85	1	11.85	1.86	0.1928	
<b>Residual</b>	95.63	15	6.38			
Lack of Fit	70.9	10	7.09	1.43	0.3627	not significant
Pure Error	24.74	5	4.95			
<b>Cor Total</b>	2031.42	29				

These values (Adjusted  $R^2$  and Predicted  $R^2$ ) confirm that suggested quadratic model gives an excellent explanation for the relationship between independent factors and corresponding response [41] and the compatibility of experimental values with predicted one [84]. Adeq Precision, that measures the signal to noise ratio, was 18.4125 which also supporting the fitness of the selected model [85].

**Table 9:** Fit statistics

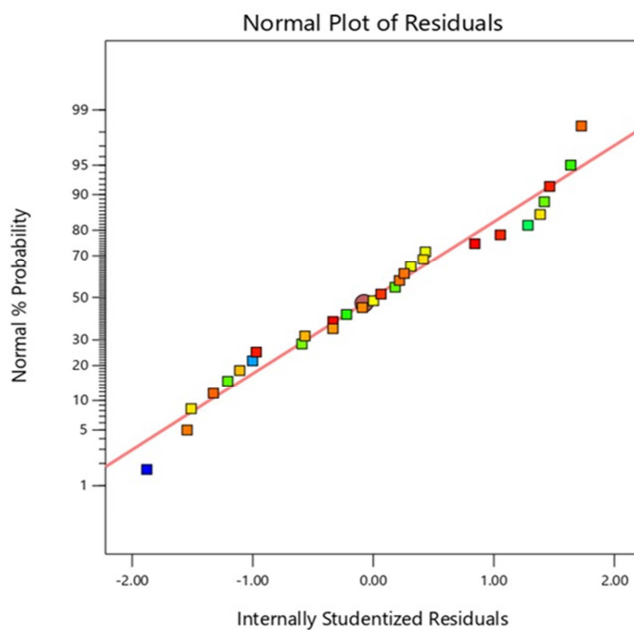
<b>Std. Dev.</b>	2.53	<b>R<sup>2</sup></b>	0.9529
<b>Mean</b>	77.93	<b>Adjusted R<sup>2</sup></b>	0.909
<b>C.V. %</b>	3.24	<b>Predicted R<sup>2</sup></b>	0.7814
		<b>Adeq Precision</b>	18.4125

The normal probability assumption of the residual was checked for its normality by plotting internally studentized residuals versus normal probability (%), as given in Fig. (7).

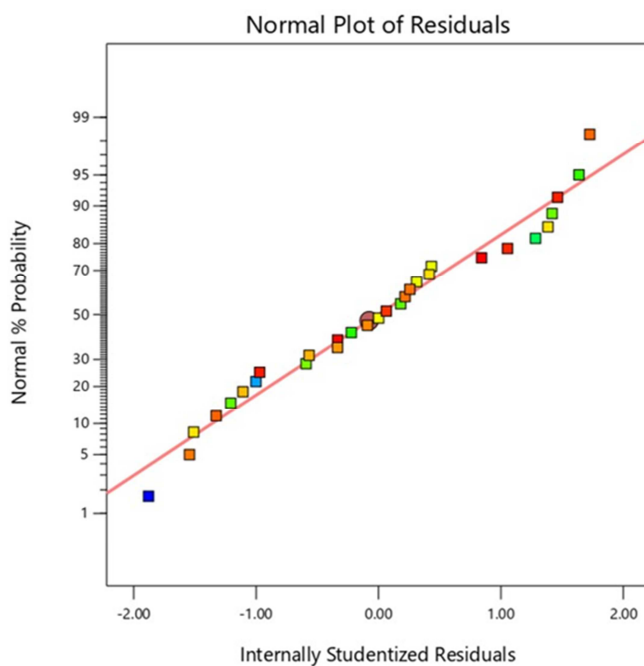
Fig. (7) shows how well the model satisfies the normality assumptions of the ANOVA where all residual plotted points are approximately close to straight line [42,86–90].

Fig. (8) shows Cook's distance plot versus run order; according to this figure all Cook's distance value were lower than 1 and there is no points that were potentially powerful due to their location in the factor, so it was concluded that the suggested model is adequate and fitted to describe the adsorption process of methylene blue by prepared nanocomposite [41,91].

Fig. (9) illustrates that the experimental and theoretical values of removal percentage are nearly similar, which is very good evidence of goodness and compatibility of the suggested quadratic model with the experimental data [91].



**Figure 7:** Normal plot of probability (%) versus internally studentized residuals



**Figure 8:** Plot of Cook's distance vs run order

The effects of various independent variables in terms of 2D contour plots and 3D surface plots are illustrated in Fig. (10a–f). In these plots, the effect of four independent factors on the removal process will be investigated simultaneously.



**Figure 9:** Diagnostic plots of the comparison between predicted and actual values of removal process of MB dye using the prepared nanocomposite.

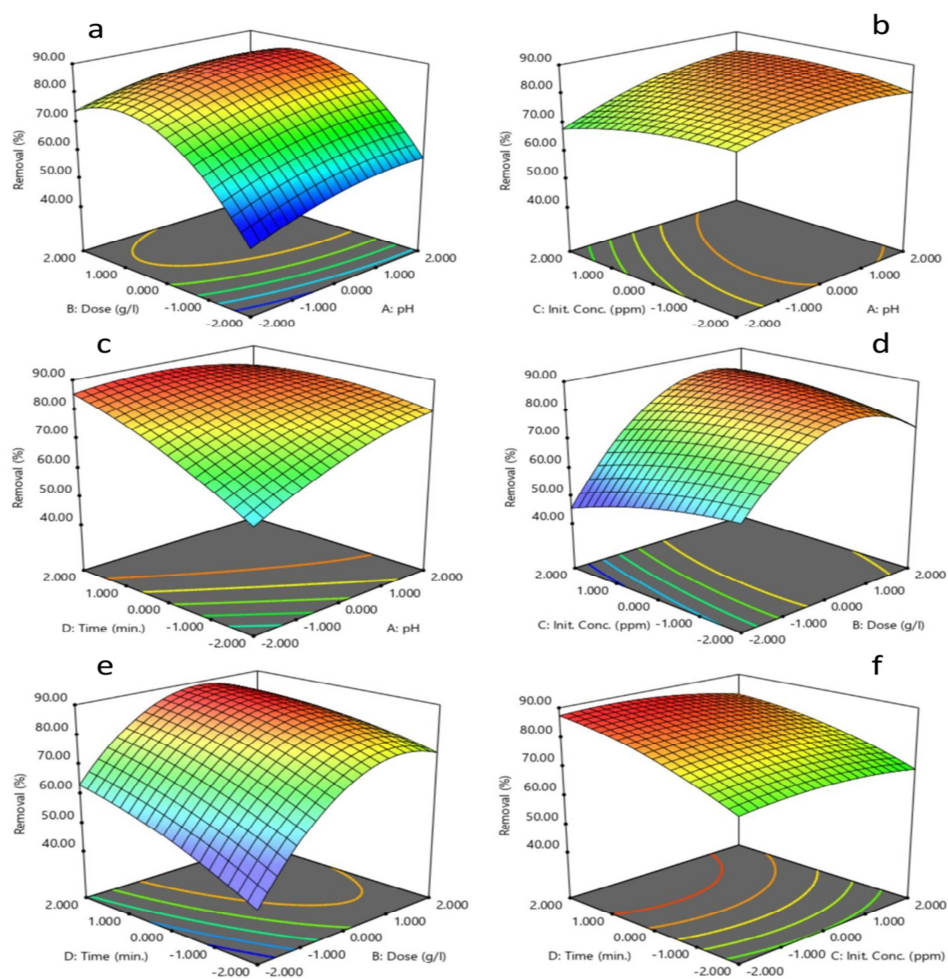


**Figure 10:** 2D contour and 3D surface plots of the various effects of different independent variables on the removal process of MB using the prepared nanocomposite.

#### 4. Conclusion

A novel sediment–alga–silver nanocomposite was developed for the elimination of MB dye from aqueous solutions. An economic and ecofriendly approach for the green synthesis of AgNPs utilizing the red alga *J. rubens* was applied. The resulting nanoparticles were then used for the synthesis of sediment–alga–silver nanocomposite. Experimental results were well-fitted to both the Langmuir ( $R^2 = 0.9915$ ) and Freundlich ( $R^2 = 0.9991$ ) isotherm models. The kinetics of the process demonstrated that the pseudo-second-order model effectively characterizes the physisorption kinetics of MB. Results from the factorial experimental design indicated that pH and adsorbent dosage were the most effective factors influencing the removal efficiency. The design revealed matching of the experimental and theoretical removal percentages, providing strong evidence for the suggested quadratic model's goodness and its compatibility with the experimental data. The obtained results are very promising because the sediment–alga–silver nanocomposite effectively removed the MB dye. Further, this nanocomposite is a compelling, eco-friendly, low-cost, and readily available material. It could be a viable alternative to more costly adsorbents commonly utilized for MB elimination.

#### Statements and Declarations

**Funding:** The authors have no relevant financial or non-financial interests to disclose.

**Conflicts of interest/Competing interests:** The authors have no competing interests to declare that are relevant to the content of this article.

#### 5. References

- [1] A.M. Elgarahy, H.Y. Mostafa, E.G. Zaki, S.M. ElSaeed, K.Z. Elwakeel, A. Akhdhar, E. Guibal, Methylene blue removal from aqueous solutions using a biochar/gellan gum hydrogel composite: Effect of agitation mode on sorption kinetics, *Int. J. Biol. Macromol.* 232 (2023) 123355. <https://doi.org/10.1016/j.ijbiomac.2023.123355>.
- [2] A. Ayub, Z.A. Raza, M.I. Majeed, M.R. Tariq, A. Irfan, Development of sustainable magnetic chitosan biosorbent beads for kinetic remediation of arsenic contaminated water, *Int. J. Biol. Macromol.* 163 (2020) 603–617. <https://doi.org/10.1016/j.ijbiomac.2020.06.287>.
- [3] K.N. Palansooriya, Y. Yang, Y.F. Tsang, B. Sarkar, D. Hou, X. Cao, E. Meers, J. Rinklebe, K.-H. Kim, Y.S. Ok, Occurrence of contaminants in drinking water sources and the potential of biochar for water quality improvement: A review, *Crit. Rev. Environ. Sci. Technol.* 50 (2020) 549–611. <https://doi.org/10.1080/10643389.2019.1629803>.
- [4] M.T. Yagub, T.K. Sen, S. Afroze, H.M. Ang, Dye and its removal from aqueous solution by adsorption: A review, *Adv. Colloid Interface Sci.* 209 (2014) 172–184. <https://doi.org/10.1016/j.cis.2014.04.002>.
- [5] X.-S. Hu, R. Liang, G. Sun, Super-adsorbent hydrogel for removal of methylene blue dye from aqueous solution, *J. Mater. Chem. A* 6 (2018) 17612–17624. <https://doi.org/10.1039/C8TA04722G>.
- [6] F.T. Alshorifi, S.L. Ali, R.S. Salama, Promotional synergistic effect of Cs–Au NPs on the performance of Cs–Au/MgFe<sub>2</sub>O<sub>4</sub> catalysts in catalysis 3,4-dihydropyrimidin-2(1H)-ones and degradation of RhB dye, *J. Inorg. Organomet. Polym. Mater.* 32 (2022) 3765–3776. <https://doi.org/10.1007/s10904-022-02389-8>.
- [7] S. Laurent, D. Forge, M. Port, A. Roch, C. Robic, L. Vander Elst, R.N. Muller, Magnetic iron oxide nanoparticles: synthesis, stabilization, vectorization, physicochemical characterizations, and biological applications, *Chem. Rev.* 108 (2008) 2064–2110. <https://doi.org/10.1021/cr068445e>.
- [8] C. Li, H. Liu, X. Jiang, G.I.N. Waterhouse, Z. Zhang, L. Yu, Hierarchical Fe<sub>3</sub>O<sub>4</sub>/C with a flower-like morphology: A highly efficient and reusable dye adsorbent, *Synth. Met.* 246 (2018) 45–56. <https://doi.org/10.1016/j.synthmet.2018.09.010>.
- [9] P.M. Thabede, N.D. Shooto, E.B. Naidoo, Removal of methylene blue dye and lead ions from aqueous solution using activated carbon from black cumin seeds, *South African J. Chem. Eng.* 33 (2020) 39–50. <https://doi.org/10.1016/j.sajce.2020.04.002>.
- [10] Y. Li, Y. An, R. Zhao, Y. Zhong, S. Long, J. Yang, J. Li, H. Zheng, Synergetic removal of oppositely charged dyes by co-precipitation and amphoteric self-floating capturer: Mechanism investigation by molecular simulation, *Chemosphere* 296 (2022) 134033. <https://doi.org/10.1016/j.chemosphere.2022.134033>.
- [11] G. Han, Y. Du, Y. Huang, W. Wang, S. Su, B. Liu, Study on the removal of hazardous Congo red from aqueous solutions by chelation flocculation and precipitation flotation process, *Chemosphere* 289 (2022) 133109. <https://doi.org/10.1016/j.chemosphere.2021.133109>.
- [12] M. Liu, W. Yin, T.-L. Zhao, Q.-Z. Yao, S.-Q. Fu, G.-T. Zhou, High-efficient removal of organic dyes from model wastewater using Mg(OH)<sub>2</sub>-MnO<sub>2</sub> nanocomposite: synergistic effects of adsorption, precipitation, and photodegradation, *Sep. Purif. Technol.* 272 (2021) 118901. <https://doi.org/10.1016/j.seppur.2021.118901>.
- [13] L. Villar Blanco, O. González Sas, P.B. Sánchez, Á. Domínguez Santiago, B. González de Prado, Congo red recovery from water using green extraction solvents, *Water Resour. Ind.* 27 (2022) 100170. <https://doi.org/10.1016/j.wri.2021.100170>.
- [14] L. Bukman, V.R. De Souza, N.R.C. Fernandes, W. Caetano, V.R. Batistela, N. Hioka, Reverse micellar extraction of dyes based on fatty acids and recoverable organic solvents, *Sep. Purif. Technol.* 242 (2020) 116772. <https://doi.org/10.1016/j.seppur.2020.116772>.
- [15] S. Yi, G. Sun, F. Dai, Removal and separation of mixed ionic dyes by solvent extraction, *Text. Res. J.* 88 (2018) 1641–1649. <https://doi.org/10.1177/0040517517705631>.
- [16] Y. Wang, W. Zhang, M. Qin, M. Zhao, Y. Zhang, Green one-pot preparation of  $\alpha$ -Fe<sub>2</sub>O<sub>3</sub>@carboxyl-functionalized yeast composite with high adsorption and catalysis properties for removal of methylene blue, *Surf. Interface Anal.* 50 (2018) 311–320. <https://doi.org/10.1002/sia.6370>.
- [17] O. Długosz, A. Staroń, P. Brzoza, M. Banach, Synergistic effect of sorption and photocatalysis on the degree of dye removal in single and multicomponent systems on ZnO-SnO<sub>2</sub>, *Environ. Sci. Pollut. Res.* 29 (2022) 27042–27050.

- <https://doi.org/10.1007/s11356-021-18044-7>.
- [18] R.H. Thabet, M.K. Fouad, I.A. Ali, S.A. El Sherbiny, M.A. Tony, Synthesis, characterization and potential application of magnetized nanoparticles for photocatalysis of Levafix CA reactive azo-dye in aqueous effluent. *Water Environ. J.* 36 (2022) 245–260. <https://doi.org/10.1111/wej.12756>.
- [19] C. Osagie, A. Othmani, S. Ghosh, A. Malloum, Z. Kashitarash Esfahani, S. Ahmadi, Dyes adsorption from aqueous media through the nanotechnology: A review, *J. Mater. Res. Technol.* 14 (2021) 2195–2218. <https://doi.org/10.1016/j.jmrt.2021.07.085>.
- [20] S. Sahoo, Uma, S. Banerjee, Y.C. Sharma, Application of natural clay as a potential adsorbent for the removal of a toxic dye from aqueous solutions, *Desalin. Water Treat.* 52 (2014) 6703–6711. <https://doi.org/10.1080/19443994.2013.816872>.
- [21] A. Ouakouak, M. Abdelhamid, B. Thouraya, H.-O. Chahinez, G. Hocine, N. Hamdi, A. Syafiuddin, R. Boopathy, Development of a novel adsorbent prepared from dredging sediment for effective removal of dye in aqueous solutions, *Appl. Sci.* 11 (2021) 10722. <https://doi.org/10.3390/app112210722>.
- [22] S.I. Al-Saeedi, A. Areej, M.T. Qamar, A. Alhujaily, S. Iqbal, M.T. Alotaibi, M. Aslam, M.A. Qayyum, A. Bahadur, N.S. Awwad, Y. Jazaa, E.B. Elkhaed, Isotherm and kinetic studies for the adsorption of methylene blue onto a novel Mn<sub>3</sub>O<sub>4</sub>-Bi<sub>2</sub>O<sub>3</sub> composite and their antifungal performance, *Front. Environ. Sci.* 11 (2023) 1156475. <https://doi.org/10.3389/fenvs.2023.1156475>.
- [23] A.T. Mansour, A.E. Alprol, K.M. Abualnaja, H.S. El-Beltagi, K.M.A. Ramadan, M. Ashour, Dried brown seaweed's phytoremediation potential for methylene blue dye removal from aquatic environments, *Polymers.* 14 (2022) 1375. <https://doi.org/10.3390/polym14071375>.
- [24] M. Yadav, S. Thakore, R. Jadeja, Removal of organic dyes using *Fucus vesiculosus* seaweed bioadsorbent an ecofriendly approach: Equilibrium, kinetics and thermodynamic studies, *Environ. Chem. Ecotoxicol.* 4 (2022) 67–77. <https://doi.org/10.1016/j.enceco.2021.12.003>.
- [25] K. Sharma, S. Sharma, V. Sharma, P.K. Mishra, A. Ekielski, V. Sharma, V. Kumar, Methylene blue dye adsorption from wastewater using hydroxyapatite/gold nanocomposite: kinetic and thermodynamics Studies, *Nanomaterials* 11 (2021) 1403. <https://doi.org/10.3390/nano11061403>.
- [26] I.M. Minisy, N.A. Salahuddin, M.M. Ayad, Adsorption of methylene blue onto chitosan–montmorillonite/polyaniline nanocomposite, *Appl. Clay Sci.* 203 (2021) 105993. <https://doi.org/10.1016/j.clay.2021.105993>.
- [27] M.K. Satapathy, P. Das, Optimization of crystal violet dye removal using novel soil-silver nanocomposite as nanoadsorbent using response surface methodology, *J. Environ. Chem. Eng.* 2 (2014) 708–714. <https://doi.org/10.1016/j.jece.2013.11.012>.
- [28] P. Bhuyar, M.H.A. Rahim, S. Sundararaju, R. Ramaraj, G.P. Maniam, N. Govindan, Synthesis of silver nanoparticles using marine macroalgae *Padina* sp. and its antibacterial activity towards pathogenic bacteria, Beni-Suef Univ. *J. Basic Appl. Sci.* 9 (2020) 3–18. <https://doi.org/10.1186/s43088-019-0031-y>.
- [29] F. Geyikci, Factorial experimental design for adsorption silver ions from water onto montmorillonite, *Acta Geodyn. Geomater.* (2013) 363–370. <https://doi.org/10.13168/AGG.2013.0035>.
- [30] S. Saadat, A. Karimi-Jashni, Optimization of Pb(II) adsorption onto modified walnut shells using factorial design and simplex methodologies, *Chem. Eng. J.* 173 (2011) 743–749. <https://doi.org/10.1016/j.cej.2011.08.042>.
- [31] M.A. Aly-Eldeen, A.A.M. El-Sayed, D.M.S.A. Salem, G.M. El Zokm, The uptake of Eriochrome Black T dye from aqueous solutions utilizing waste activated sludge: Adsorption process optimization using factorial design, *Egypt. J. Aquat. Res.* 44 (2018) 179–186. <https://doi.org/https://doi.org/10.1016/j.ejar.2018.09.001>.
- [32] R. Aziam, L. Boukarma, A. Zaghoul, R. Benhiti, E. Eddaoudi, M. Zerbet, M. Chiban, Factor design methodology for modelling and optimization of carcinogenic acid dye adsorption onto Moroccan prickly pear cactus peel, *E3S Web Conf.* 240 (2021) 02005. <https://doi.org/10.1051/e3sconf/202124002005>.
- [33] K.A. Abdulsalam, B.H. Amodu, O.K. Fakorede, J.M. Adelowo, A.P. Onifade, F.C. Olowosaga, O.D. Omikunle, B. Akintayo, Optimized sorption of methyl orange using functionalized carob plant pod, *J. Chem. Soc. Niger.* 45 (2020) 1020–1026. <https://doi.org/10.46602/jcsn.v45i6.550>.
- [34] N. Özbay, A.Ş. Yargıç, R.Z. Yarbay-Şahin, E. Önal, Full factorial experimental design analysis of reactive dye removal by carbon adsorption, *J. Chem.* 2013 (2013) 234904. <https://doi.org/10.1155/2013/234904>.
- [35] A.A.M. El-Sayed, M.M. Ismail, Physico-chemodiversity variation between the most common calcareous red seaweed, Eastern Harbor, Alexandria, Egypt, *Heliyon* 8 (2022) e12457. <https://doi.org/10.1016/j.heliyon.2022.e12457>.
- [36] S.A. Abdel Ghani, M.I.A. Ibrahim, M.A. Shreadah, A.A.M. El-Sayed, M.A. Aly-Eldeen, Ecological risk assessment of selected contaminants in seawater, sediment and some fish species from Alexandria beaches, South-Eastern Mediterranean Sea, Egypt, *Environ. Nanotechnology, Monit. Manag.* 20 (2023) 100873. <https://doi.org/10.1016/j.enmm.2023.100873>.
- [37] P. Kumar, S. Senthamil Selvi, M. Govindaraju, Seaweed-mediated biosynthesis of silver nanoparticles using *Gracilaria corticata* for its antifungal activity against *Candida* spp., *Appl. Nanosci.* 3 (2013) 495–500. <https://doi.org/10.1007/s13204-012-0151-3>.
- [38] R.R.R. Kannan, R. Arumugam, D. Ramya, K. Manivannan, P. Anantharaman, Green synthesis of silver nanoparticles using marine macroalga *Chaetomorpha linum*, *Appl. Nanosci.* 3 (2013) 229–233. <https://doi.org/10.1007/s13204-012-0125-5>.
- [39] T. Handayani, Emriadi, Deswati, P. Ramadhani, R. Zein, Modelling studies of methylene blue dye removal using activated corn husk waste: Isotherm, kinetic and thermodynamic evaluation, *South African J. Chem. Eng.* 47 (2024) 15–27. <https://doi.org/10.1016/j.sajce.2023.10.003>.
- [40] H. Ouaddari, B. Abbou, I. Lebkiari, A. Habsaoui, M. Ouzzine, R. Fath Allah, Removal of Methylene Blue by adsorption onto natural and purified clays: Kinetic and thermodynamic study, *Chem. Phys. Impact* 8 (2024) 100405. <https://doi.org/10.1016/j.chphi.2023.100405>.

- [41] S. Chatteraj, N.K. Mondal, B. Das, P. Roy, B. Sadhukhan, Biosorption of carbaryl from aqueous solution onto *Pistia stratiotes* biomass, *Appl. Water Sci.* 4 (2014) 79–88. <https://doi.org/10.1007/s13201-013-0132-z>.
- [42] R.H. Myers, D.C. Montgomery, C.M. Anderson-Cook, *Response surface methodology: process and product optimization using designed experiments*, John Wiley & Sons, 2016.
- [43] J. Bensalah, A. El Amri, A. Ouass, O. Hammami, L. Kadiri, H. Ouaddari, S. El Mustapha, A. Zarrouk, A. Lebkiri, B. Srhir, E.H. Rifi, Investigation of the cationic resin Am@IRC-50 as a potential adsorbent of Co (II): Equilibrium isotherms and thermodynamic studies, *Chem. Data Collect.* 39 (2022) 100879. <https://doi.org/10.1016/j.cdc.2022.100879>.
- [44] I. Langmuir, The adsorption of gases on plane surfaces of glass, mica and platinum, *J. Am. Chem. Soc.* 40 (1918) 1361–1403. <https://doi.org/10.1021/ja02242a004>.
- [45] J. Zhang, M. Yan, G. Sun, K. Liu, An environment-friendly Fe<sub>3</sub>O<sub>4</sub>@CFAS porous ceramic: Adsorption of Cu(II) ions and process optimisation using response surface methodology, *Ceram. Int.* 47 (2021) 8256–8264. <https://doi.org/10.1016/j.ceramint.2020.11.185>.
- [46] H. Freundlich, Over the Adsorption in Solution, *J. Phys. Chem.* 57 (1906) 1100–1107. <https://www.degruyter.com/document/doi/10.1515/zpch-1907-5723/html>.
- [47] N.C. Joshi, K. Kaur, N. Kumar, N.S. Bhandari, A. Thakur, Synthesis and adsorption applications of PPY/Fe<sub>3</sub>O<sub>4</sub> nanocomposite based material, *Nano-Structures & Nano-Objects* 25 (2021) 100669. <https://doi.org/10.1016/j.nanos.2021.100669>.
- [48] A. Gamal, A.G. Ibrahim, E.M. Eliwa, A.H. El-Zomrawy, S.M. El-Bahy, Synthesis and characterization of a novel benzothiazole functionalized chitosan and its use for effective adsorption of Cu(II), *Int. J. Biol. Macromol.* 183 (2021) 1283–1292. <https://doi.org/10.1016/j.ijbiomac.2021.05.080>.
- [49] M.M. Dubinin, L.V. Radushkevich, The equation of the characteristic curve of activated charcoal., *Dokl. Akad. Nauk. SSSR* 55 (1947) 327–329.
- [50] Z. Huang, Z. Huang, L. Feng, X. Luo, P. Wu, L. Cui, X. Mao, Modified cellulose by polyethyleneimine and ethylenediamine with induced Cu(II) and Pb(II) adsorption potentialities, *Carbohydr. Polym.* 202 (2018) 470–478. <https://doi.org/10.1016/j.carbpol.2018.08.136>.
- [51] P.T. Ngueagni, E.D. Woumfo, P.S. Kumar, M. Siéwé, J. Vieillard, N. Brun, P.F. Nkuigie, Adsorption of Cu(II) ions by modified horn core: Effect of temperature on adsorbent preparation and extended application in river water, *J. Mol. Liq.* 298 (2020) 112023. <https://doi.org/10.1016/j.molliq.2019.112023>.
- [52] M.I. Temkin, Kinetics of ammonia synthesis on promoted iron catalysts, *Acta Physiochim. URSS* 12 (1940) 327–356. <https://cir.nii.ac.jp/crid/1573387451182255872> (accessed January 8, 2023).
- [53] Y.S. Ho, J.C.Y. Ng, G. McKay, Kinetics of pollutant sorption by biosorbents: review, *Sep. Purif. Methods* 29 (2000) 189–232. <https://doi.org/10.1081/SPM-100100009>.
- [54] L. Wu, W. Wan, Z. Shang, X. Gao, N. Kobayashi, G. Luo, Z. Li, Surface modification of phosphoric acid activated carbon by using non-thermal plasma for enhancement of Cu(II) adsorption from aqueous solutions, *Sep. Purif. Technol.* 197 (2018) 156–169. <https://doi.org/10.1016/j.seppur.2018.01.007>.
- [55] S.M. Anush, B. Vishalakshi, Modified chitosan gel incorporated with magnetic nanoparticle for removal of Cu(II) and Cr(VI) from aqueous solution, *Int. J. Biol. Macromol.* 133 (2019) 1051–1062. <https://doi.org/10.1016/j.ijbiomac.2019.04.179>.
- [56] Y. Ren, X. Wei, M. Zhang, Adsorption character for removal Cu(II) by magnetic Cu(II) ion imprinted composite adsorbent, *J. Hazard. Mater.* 158 (2008) 14–22. <https://doi.org/10.1016/j.jhazmat.2008.01.044>.
- [57] M. Kumari, S.K. Gupta, Response surface methodological (RSM) approach for optimizing the removal of trihalomethanes (THMs) and its precursor's by surfactant modified magnetic nanoadsorbents (sMNP) - An endeavor to diminish probable cancer risk, *Sci. Rep.* 9 (2019) 18339. <https://doi.org/10.1038/s41598-019-54902-8>.
- [58] S. Gomaa, N.M. Hilal, S.H. Abofarha, Improvement of dyeing and antimicrobial properties of cotton fabrics through pre-treatment with silver nanoparticles, *Egypt. J. Chem.* 63 (2019) 1205–1217. <https://doi.org/10.21608/ejchem.2019.13705.1846>.
- [59] S.I. Al-Saeedi, M. Ashour, A.E. Alprol, Adsorption of toxic dye using red seaweeds from synthetic aqueous solution and its application to industrial wastewater effluents, *Front. Mar. Sci.* 10 (2023) 1202362. <https://doi.org/10.3389/fmars.2023.1202362>.
- [60] A. Ibrahim, G. El Fawal, M. Akl, Methylene blue and crystal violet dyes removal (as a binary system) from aqueous solution using local soil clay: kinetics study and equilibrium isotherms, *Egypt. J. Chem.* 62 (2018) 541–554. <https://doi.org/10.21608/ejchem.2018.4113.1360>.
- [61] D. Garg, C.B. Majumder, S. Kumar, B. Sarkar, Removal of Direct Blue-86 dye from aqueous solution using alginate encapsulated activated carbon (PnsAC-alginate) prepared from waste peanut shell, *J. Environ. Chem. Eng.* 7 (2019) 103365. <https://doi.org/10.1016/j.jece.2019.103365>.
- [62] P.G. Bhavyasree, T.S. Xavier, Adsorption studies of Methylene Blue, Coomassie Brilliant Blue, and Congo Red dyes onto CuO/C nanocomposites synthesized via Vitex negundo Linn leaf extract, *Curr. Res. Green Sustain. Chem.* 4 (2021) 100161. <https://doi.org/10.1016/j.crgsc.2021.100161>.
- [63] A.T. Mansour, A.E. Alprol, K.M. Abualnaja, H.S. El-Beltagi, K.M.A. Ramadan, M. Ashour, The using of nanoparticles of microalgae in remediation of toxic dye from industrial wastewater: kinetic and isotherm studies, *Materials.* 15 (2022) 3922–3948. <https://doi.org/10.3390/ma15113922>.
- [64] H.M. El-Rafie, M.H. El-Rafie, M.K. Zahran, Green synthesis of silver nanoparticles using polysaccharides extracted from marine macro algae, *Carbohydr. Polym.* 96 (2013) 403–410. <https://doi.org/10.1016/j.carbpol.2013.03.071>.
- [65] A. El Refaey, Removal of methylene blue dye from aqueous solutions by bentonite and cement kiln dust: comparative study of adsorption equilibrium, kinetic, and thermodynamic, *Alexandria Sci. Exch. J.* 42 (2021) 629–644.



- <https://doi.org/10.21608/asejaiqsae.2021.186823>.
- [66] P. Mundada, U. Brigh, A.B. Gupta, Removal of methylene blue on soil: an alternative to clay, *Desalin. Water Treat.* 58 (2017) 267–273. <https://doi.org/10.5004/dwt.2017.0215>.
- [67] G.C. Fontes, V.M.A. Calado, A.M. Rossi, M.H.M. da Rocha-Leão, Characterization of antibiotic-loaded alginate-Osa starch microbeads produced by ionotropic pregelation, *Biomed Res. Int.* 2013 (2013) 472626. <https://doi.org/10.1155/2013/472626>.
- [68] E.A. Mandhour, Validity of sand dunes sediments as a fine aggregates for roads works: a case study on sand dunes sediments, Al-Nasiriya city, southern Iraq, *Period. Eng. Nat. Sci.* 8 (2020) 849–858.
- [69] A. Nuzzo, P. Buurman, V. Cozzolino, R. Spaccini, A. Piccolo, Infrared spectra of soil organic matter under a primary vegetation sequence, *Chem. Biol. Technol. Agric.* 7 (2020) 6. <https://doi.org/10.1186/s40538-019-0172-1>.
- [70] R.S. Raubbin, R.L. Laju, P. Ambika, A. Pushparaj, HPLC, FTIR and GC-MS analysis of ethyl acetate extract of red seaweed *hypnea flagelliformis* graville ex j. Agardh 1851, *Int. J. Pharm. Sci. Res.* 11 (2020) 3953–3959. [https://doi.org/10.13040/IJPSR.0975-8232.11\(8\).3953-59](https://doi.org/10.13040/IJPSR.0975-8232.11(8).3953-59).
- [71] Y.S. Ng, B. Sen Gupta, M.A. Hashim, Performance evaluation of natural iron-rich sandy soil as a low-cost adsorbent for removal of lead from water, *Desalin. Water Treat.* 57 (2016) 5013–5024. <https://doi.org/10.1080/19443994.2014.999711>.
- [72] T. Ainane, F. Khammour, M. Talbi, M. Elkouali, A novel bio-adsorbent of mint waste for dyes remediation in aqueous environments: study and modeling of isotherms for removal of methylene Blue, *Orient. J. Chem.* 30 (2014) 1183–1189. <https://doi.org/10.13005/ojc/300332>.
- [73] K. Bhattacharyya, A. Sharma, Kinetics and thermodynamics of Methylene Blue adsorption on Neem (*Azadirachta indica*) leaf powder, *Dye. Pigment.* 65 (2005) 51–59. <https://doi.org/10.1016/j.dyepig.2004.06.016>.
- [74] R.-L. Tseng, S.-K. Tseng, F.-C. Wu, Preparation of high surface area carbons from Corn cob with KOH etching plus CO<sub>2</sub> gasification for the adsorption of dyes and phenols from water, *Colloids Surfaces A Physicochem. Eng. Asp.* 279 (2006) 69–78. <https://doi.org/10.1016/j.colsurfa.2005.12.042>.
- [75] S. Goldberg, Equations and Models Describing Adsorption Processes in Soils, in: Soil Science Society of America, Inc. Madison, Wisconsin, USA, 2005.
- [76] O.S. Bello, O.M. Adelaide, M.A. Hamed, O.A.M. Popoola, Kinetic and equilibrium studies of methylene blue removal from aqueous solution by adsorption on treated sawdust, *Maced. J. Chem. Chem. Eng.* 29 (2010) 77. <https://doi.org/10.20450/mjce.2010.181>.
- [77] B.K. Bindhu, H. Shaji, K.J. Kuruvila, M. Nazerine, S. Shaji, Removal of total hardness using low cost adsorbents, *IOP Conf. Ser. Mater. Sci. Eng.* 1114 (2021) 012089. <https://doi.org/10.1088/1757-899X/1114/1/012089>.
- [78] R.K. Ameta, [Fe(CN)<sub>6</sub>NO]<sup>2-</sup>-Based MOIFs for adsorption of organic pollutants and as a self-rotatory motor, *ACS Omega* 6 (2021) 456–464. <https://doi.org/10.1021/acsomega.0c04896>.
- [79] Z.-Y. Zhong, Q. Yang, X.-M. Li, K. Luo, Y. Liu, G.-M. Zeng, Preparation of peanut hull-based activated carbon by microwave-induced phosphoric acid activation and its application in Remazol Brilliant Blue R adsorption, *Ind. Crops Prod.* 37 (2012) 178–185. <https://doi.org/10.1016/j.indcrop.2011.12.015>.
- [80] S. Boddu, J.B. Dulla, V.N. Alugunulla, A.A. Khan, An assessment on removal performance of arsenic with treated *Turbinaria vulgaris* as an adsorbent: characterization, optimization, isotherm, and kinetics study, *Environ. Prog. Sustain. Energy* 39 (2020) e13313. <https://doi.org/10.1002/ep.13313>.
- [81] C. Theivarasu, S. Mylsamy, Equilibrium and Kinetic adsorption studies of Rhodamine-B from aqueous solutions using cocoa (Theobroma cacao) s hell as a new adsorbent, *Int. J. Eng. Sci. Technol.* 2 (2010) 6284–6292.
- [82] H. Ahmadi, A. Rajaei, M. Nayeripour, M.G. Varzaneh, A hybrid control method to improve LVRT and FRT in DFIG by using the multi-objective algorithm of krill and the fuzzy logic, *Iran. J. Electr. Electron. Eng.* 14 (2018) 330–341. <https://doi.org/10.22068/IJEEE.14.4.330>.
- [83] C.A. Igwegbe, L. Mohammadi, S. Ahmadi, A. Rahdar, D. Khadkhodai, R. Dehghani, S. Rahdar, Modeling of adsorption of Methylene Blue dye on Ho-CaWO<sub>4</sub> nanoparticles using Response Surface Methodology (RSM) and Artificial Neural Network (ANN) techniques, *MethodsX* 6 (2019) 1779–1797. <https://doi.org/10.1016/j.mex.2019.07.016>.
- [84] R. Najeeb, A. Abbar, Optimization of COD Removal from pharmaceutical wastewater by electrocoagulation process using Response Surface Methodology (RSM), *Egypt. J. Chem.* 65 (2022) 619–631. <https://doi.org/10.21608/ejchem.2021.82809.4107>.
- [85] R.L. Mason, R.F. Gunst, J.L. Hess, *Statistical Design and Analysis of Experiments*, 2nd editio, Wiley, 2003. <https://doi.org/10.1002/0471458503>.
- [86] S. Di Leo, P. Caramuta, P. Curci, C. Cosmi, Regression analysis for energy demand projection: An application to TIMES-Basilicata and TIMES-Italy energy models, *Energy* 196 (2020) 117058. <https://doi.org/10.1016/j.energy.2020.117058>.
- [87] K. Raja, V.S. Chandra Sekar, V. Vignesh Kumar, T. Ramkumar, P. Ganeshan, Microstructure characterization and performance evaluation on AA7075 metal matrix composites using RSM technique, *Arab. J. Sci. Eng.* 45 (2020) 9481–9495. <https://doi.org/10.1007/s13369-020-04752-8>.
- [88] Y. Rostamiyan, A. Hamed Mashhadzadeh, A. SalmanKhani, Optimization of mechanical properties of epoxy-based hybrid nanocomposite: Effect of using nano silica and high-impact polystyrene by mixture design approach, *Mater. Des.* 56 (2014) 1068–1077. <https://doi.org/10.1016/j.matdes.2013.11.060>.
- [89] B.K. Körbahti, M.A. Rauf, Application of response surface analysis to the photolytic degradation of Basic Red 2 dye, *Chem. Eng. J.* 138 (2008) 166–171. <https://doi.org/10.1016/j.cej.2007.06.016>.
- [90] D.C. Montgomery, *Design and Analysis of Experiments*, 4th Editio, Wiley, 1996.
- [91] K. Oktor, N.Y. Yuzer, G. Hasirci, N. Hilmioglu, Optimization of removal of phosphate from water by adsorption using biopolymer chitosan beads, *Water, Air, Soil Pollut.* 234 (2023) 271. <https://doi.org/10.1007/s11270-023-06230-x>.